

# Protons in the Near Lunar Wake Observed by the SARA Instrument on Board Chandrayaan-1

Y. Futaana,<sup>1</sup> S. Barabash,<sup>1</sup> M. Wieser,<sup>1</sup> M. Holmström,<sup>1</sup> A. Bhardwaj,<sup>2</sup> M. B. Dhanya,<sup>2</sup> R. Sridharan,<sup>2</sup> P. Wurz,<sup>3</sup> A. Schaufelberger,<sup>3</sup> K. Asamura<sup>4</sup>

---

Y. Futaana, Swedish Institute of Space Physics, Box 812, Kiruna, SE-98128, Sweden.  
(futaana@irf.se)

<sup>1</sup> Swedish Institute of Space Physics, Box 812, Kiruna, SE-98128, Sweden

<sup>2</sup> Space Physics Laboratory, Vikram Sarabhai Space Center, Trivandrum 695 022, India

<sup>3</sup> Physikalisches Institut, University of Bern, Sidlerstrasse 5, CH-3012 Bern, Switzerland

<sup>4</sup> Institute of Space and Astronautical Science, 3-1-1 Yoshinodai, Sagamihara, Japan

## Index Terms

6250 Moon

5421 Interactions with particles and fields

2780 Magnetospheric Physics: Solar wind interactions with unmagnetized bodies

7807 Space Plasma Physics: Charged particle motion and acceleration

## Abstract

Significant proton fluxes were detected in the near wake region of the Moon by an ion mass spectrometer on board Chandrayaan-1. The energy of these nightside protons is slightly higher than the energy of the solar wind protons. The protons are detected close to the lunar equatorial plane at a 140° solar zenith angle, i.e., ~50° behind the terminator at a height of 100 km. The protons come from just above the local horizon, and move along the magnetic field in the solar wind reference frame. We compared the observed proton flux with the predictions from analytical models of an electrostatic plasma expansion into a vacuum. The observed velocity was higher than the velocity predicted by analytical models by a factor of 2 to 3. The simple analytical models cannot explain the observed ion dynamics along the magnetic field in the vicinity of the Moon.

## 29 **1. Introduction**

30 The classical picture of the Moon-solar wind interaction is straightforward. Because the  
31 surface of the Moon is covered by non-conductive porous regolith, it behaves as a perfect absorber  
32 of the solar wind ions and electrons. The perturbations of lunar origin in the interplanetary magnetic  
33 field are extremely small, and therefore no significant effects are expected in the upstream solar  
34 wind. For example, no global scale bow shock is predicted, and consistently has never been  
35 observed. Only strongly, but locally, magnetized regions of crustal origin (often called magnetic  
36 anomalies) can interact with the solar wind under specific configurations, forming mini-  
37 magnetospheres (e.g., *Russell and Lichtenstein [1975]; Lin et al. [1998]; Wieser et al. [2010]*).

38 Because the supersonic solar wind plasma is largely absorbed by the dayside surface, a  
39 vacuum region is formed on the nightside of the Moon. The solar wind plasma refills the vacuum  
40 region, and corresponding ion signatures were observed during the wake crossings by WIND  
41 spacecraft in 1994 (*Ogilvie et al. [1996]*). One conclusion from these observations was that a large  
42 electric potential drop of  $\sim 400\text{V}$  close to the wake boundary has to be assumed to explain the ion  
43 signatures. Following the observations by WIND, observations of electrons and protons in the  
44 vicinity of the Moon from other missions also suggest that the significant electric potential drop  
45 does exist across the boundary (e.g., *Futaana et al. [2001]; Halekas et al. [2005]; Nishino et al.*  
46 *[2009a]*). A number of numerical simulations using particle-in-cell models and hybrid models of  
47 the solar wind-Moon interactions have been performed (*Farrell et al. [1998]; Birch and Chapman*  
48 *[2001]; Kallio [2005]; Trávníček et al. [2005]*), but the large potential drop has not been  
49 reproduced. *Halekas et al. [2005]* proposed a theory to explain the large potential drop by  
50 considering supra-thermal solar wind electrons.

51 Apart from the fluid considerations of the plasma in the vicinity of the Moon, kinetic effects  
52 have also been discussed. Using Apollo observations, *Freeman [1972]* found fluxes of light ions

53 with mass per charge less than 10 amu/q from the zenith direction in the deep wake, but the source  
54 of these light ions was not clear. *Futaana et al. [2003]* reported non-solar wind protons with ring-  
55 like velocity distribution functions during a lunar swing-by of the Nozomi spacecraft. They  
56 interpreted that those protons are most probably reflected from a local bow shock formed in front of  
57 the lunar mini-magnetosphere, but *Holmström et al. [2010]* argued that the reflected protons from  
58 the lunar surface discovered by *Saito et al. [2008]* may also explain the Nozomi observations.

59 In this paper, we report on the detection of a proton flux in the deep lunar wake region by the  
60 Sub-keV Atom Reflection Analyzer (SARA) on board Chandrayaan-1. Earlier, Nishino et al.  
61 [2009a; 2009b] identified two types of proton intrusions into the wake in the ion data obtained from  
62 the Kaguya spacecraft. However, the arrival direction of proton fluxes reported in this paper is  
63 significantly different from the fluxes reported in Nishino et al. [2009a; 2009b]. The proton  
64 population discussed here is frequently seen in the SARA data, however, we selected one particular  
65 event on 25 January, 2009 when the interplanetary magnetic field and upstream condition were  
66 stable and optimal for observations, such that the interplanetary magnetic field vector was in the  
67 ecliptic plane, and perpendicular to the solar wind velocity vector.

## 68 **2. Instrumentation**

69 The SARA data discussed in this paper were collected on a lunar polar orbit at a height of  
70 ~100 km. SARA is composed of two sensors (*Bhardwaj et al. [2005]*; *Barabash et al. [2009]*). One  
71 of the sensors is called Chandrayaan-1 Energetic Neutrals Analyzer (CENA), which is the first-ever  
72 energetic neutral atom (ENA) sensor flown to the Moon. The other sensor is Solar Wind Monitor  
73 (SWIM), an ion mass analyzer to monitor the solar wind and to study the ion environment around  
74 the Moon. Only data obtained by the SWIM sensor are used in this study.

75 The SWIM sensor is a compact electrostatic ion mass analyzer with a fan-shaped aperture  
 76 ( $\sim 7^\circ \times 160^\circ$ ) and an angular resolution of  $\sim 7^\circ \times 10^\circ$  (depending on the looking direction). The number  
 77 of angular pixels is 16 (maximum). For this study SWIM was operated with an energy range of  
 78  $\sim 100$  to  $3000$  eV/q covered by 16 logarithmically separated energy-per-charge bins. SWIM also has  
 79 a moderate mass resolution of  $m/\Delta m \sim 2$  (McCann et al. [2007]; Barabash et al. [2009]).

80 Figure 1 shows the SWIM and CENA fields of views (FoVs). The SWIM bore sight is along  
 81 the  $+z_{sc}$ -axis, and the aperture plane is perpendicular to the  $y_{sc}$ -axis. Here the subscript SC denotes  
 82 the spacecraft reference frame. The nominal spacecraft attitude is the nadir pointing. During nadir  
 83 pointing, the  $+x_{sc}$  axis always points toward the lunar surface. The velocity vector of the spacecraft  
 84 is nominally along either the  $+y_{sc}$  or the  $-y_{sc}$ -axis. During the period of the observation discussed in  
 85 this paper, the  $-y_{sc}$ -axis was co-aligned with the velocity vector. As seen in Figure 1, the SWIM  
 86 aperture is perpendicular to the spacecraft velocity vector, and some of the SWIM angular sensors  
 87 (CH-0 to -5) point toward the lunar surface. This configuration means that Chandrayaan-1 can be  
 88 considered as a spinning satellite revolving around the  $z_{sc}$ -axis with a rotation period equal to the  
 89 spacecraft orbit around the Moon ( $\sim 118$  min). The SWIM FoV plane (the half-plane of  $\pm x_{sc}$  and  
 90  $+z_{sc}$ ) can cover  $\sim 2\pi$  angular space (half hemisphere) in half of the orbital period ( $\sim 59$  min). The  
 91 three-dimensional (3-D) velocity distribution function of the solar wind can be measured only when  
 92 the spacecraft is at the dayside and the SWIM FoV is close to the ecliptic plane. Therefore, the solar  
 93 wind can be observed only once per orbit when the spacecraft is close to the lunar dayside equator.  
 94 The 3-D velocity distribution of the protons allows us to calculate the density. We calculated the  
 95 density of the protons by numerical integration over the observed flux.

96 In this paper, the lunar-centric solar ecliptic (LSE) coordinate system is used. The Moon-Sun  
 97 line is the  $+x$  axis, the velocity vector of the Sun motion relative to the Moon is the  $+y$  axis, and the  
 98  $+z$  axis completes the right-handed system. Indeed, the differences of the axis directions with the

99 geocentric solar ecliptic (GSE) frame (+ $x$  axis is the Earth-Sun line, + $z$  axis is normal to the mean  
100 ecliptic plane of the Earth pointing to north, and + $y$  axis completes the right-handed system) is in  
101 general very small ( $<0.3^\circ$ ), and it was  $\sim 0.18^\circ$  for the day of the observation.

### 102 3. Observation

103 Figure 2 shows the energy-time spectrogram of ion counts observed by SWIM on 25 January  
104 2009. The lunar phase was 2 days before the new Moon. Because the Moon was in the undisturbed  
105 solar wind, no effects from the Earth's bow shock or magnetosphere were expected. Figure 3 shows  
106 the Chandrayaan-1 orbit corresponding to the SWIM observations discussed here (orbit 942). The  
107 motion of the spacecraft was from north to south on the dayside, and from south to north on the  
108 nightside. The Sun aspect angle, the angle between the spacecraft orbital plane and Sun-Moon line,  
109 was  $\sim 40^\circ$ .

110 In the SWIM data shown in Figure 2, five distinct populations of ions, labeled as (A)-(E), can  
111 be clearly identified. The strongest flux is from the solar wind protons with an energy of  $\sim 500$ - $600$   
112 eV/ $q$  (population A). The corresponding solar wind velocity is  $\sim 310$ - $340$  km/s. At the same time,  
113 we can see the population (B) at a slightly higher energy range ( $E/q \sim 1$  keV/ $q$ ) that consists of the  $\alpha$ -  
114 particles from the solar wind. Because the  $\alpha$ -particles are doubly charged, the actual energy is  $\sim 2$   
115 keV, and the velocity was similar to that of the solar wind protons (A). These two populations are  
116 observed on the lunar dayside close to the lunar equator from directions 11 and 12, as expected.

117 The ion populations (C) and (D) are also detected on the dayside. Both populations are  
118 composed of protons as established by mass analysis (not shown here). The population (C) comes  
119 from the surface and has a broadened energy spectrum. These ions are backscattered protons from  
120 the lunar surface similar to the observations reported by *Saito et al. [2008]*. Ions of population (D)  
121 are the backscattered protons accelerated by the convection electric field of the ambient solar wind

122 electric field, which was also suggested by *Saito et al. [2008]*. Note that the accelerated protons (D)  
123 are absent on the second orbit. The signatures of this population will be discussed in the Discussion  
124 section.

125 The population (E) is a faint proton flux that can be seen in the deep nightside region. The  
126 energy of the population (E) is 0.5 to 1 keV, which is slightly higher than that of the solar wind. The  
127 densities of the solar wind (A) and the population (E) can be calculated by the integration of the  
128 observed flux. The density is  $1.7 \text{ cm}^{-3}$  for the solar wind (A) and  $(3-4) \times 10^{-3} \text{ cm}^{-3}$  for the population  
129 (E). Notably, the density calculation is not straightforward especially for the case of low ion flux,  
130 and therefore a large ambiguity may be included. In addition, the solar wind density is an  
131 underestimation because anomalously lower efficiencies than the ground calibration were found in  
132 the solar wind channels of the sensor. This is consistent with the solar wind density of 6-8/cc  
133 obtained from WIND/SWE instrument during this period. On the other hand, no such lower  
134 efficiencies were found in the channels where the population (E). The density ratio between the  
135 night side ions and the solar wind is then  $(0.5-2) \times 10^{-3}$ . As mentioned in the Instrumentation section,  
136 SWIM can measure 3-D distribution functions with the help of the spacecraft motion and its  
137 pointing. In addition, because the ion populations (A) and (E) are both narrow beams with thermal  
138 extents of  $\sim 10^\circ$  (FWHM), as estimated from the velocity spread, almost all of these beams can even  
139 be measured at a specific time.

140 ACE magnetic field data corrected for the propagation time to the Moon were used in this  
141 study to understand the interplanetary magnetic field (IMF) condition at the Moon. The separation  
142 between ACE and the Moon was  $\sim 180 R_E$  during the observations, where  $R_E$  is the Earth radius  
143 (6378 km). Considering the velocity of the solar wind of 310 to 340 km/s as observed by SWIM,  
144 the solar wind propagation between ACE and the Moon was 56 to 61 minutes. Hence, we have  
145 assumed that the time difference from ACE to the Moon was 1 hour. Figure 4 shows the

146 interplanetary magnetic field data observed by ACE in the GSE coordinate system. The difference  
 147 between the GSE and the LSE frame is small ( $\sim 0.18^\circ$ ) enough to consider them as identical. The  
 148 ACE data obtained between 12:00-18:00 UT (lower axis) were shifted to 13:00-19:00 UT at the  
 149 Moon (upper axis). The magnitude of the IMF was stable at 3-4 nT over the period of interest. The  
 150 magnetic field vector elevation angle,  $\sin^{-1}(B_z/B)$ , was almost zero, which means that the magnetic  
 151 field vector was closely confined to the  $x_{LSE}-y_{LSE}$  plane during the observations. The azimuthal  
 152 angle,  $\tan^{-1}(B_y/B_x)$ , was  $135^\circ$  before 13:00 UT ( $\sim 14:00$  UT at Moon) following the Parker spiral.  
 153 Between 13:00 and 14:00 UT (14:00 and 15:00 UT at Moon), a slightly fluctuating IMF azimuthal  
 154 angle was observed. Afterward, the angle changed to  $90^\circ$ , meaning that the IMF direction was  
 155 almost perpendicular to the solar wind velocity during the time the proton population (E) was  
 156 observed.

## 157 4. Discussion

158 The IMF configuration and the change of its direction can consistently explain the  
 159 characteristics of the accelerated protons (D). Because the direction of the convective electric field  
 160 ( $-\mathbf{v} \times \mathbf{B}$ ) points toward the northern hemisphere throughout the observations, it is natural that the  
 161 accelerated protons (D) are only detected in the northern hemisphere (Figure 2). The convective  
 162 electric field is  $\mathbf{E} = -\mathbf{v} \times \mathbf{B} = \sim 300 \text{ km/s} \times 3 \text{ nT} \times \cos 45^\circ = \sim 0.6 \text{ mV/m} = \sim 1.1 \text{ kV}/R_M$  where  $R_M$  is the  
 163 lunar radius (1738 km). The estimated energy is consistent with the observed energy of the  
 164 accelerated protons. The change in the IMF direction at 15:00 UT at the Moon can explain the  
 165 disappearance of the proton flux (D) on the second orbit. For the first orbit, the azimuthal angle of  
 166 the magnetic field ( $\tan^{-1}(B_y/B_x)$ ) was  $\sim 135^\circ$  to the Sun-Moon line. This angle means that the  
 167 magnetic field direction was almost in the same plane as the orbital plane of Chandrayaan-1 (Figure  
 168 5). The backscattered protons are accelerated by the electric field, and then start gyrating around the  
 169 magnetic field (Holmström et al., 2010). This  $\mathbf{E} \times \mathbf{B}$ -drift motion is confined in the plane

170 perpendicular to the IMF and the orbital plane in this case. Because the SWIM FoVs are  
171 perpendicular to the orbital plane, the ion gyration plane is favorable to be observed by SWIM.  
172 After the magnetic field direction changed to  $90^\circ$  prior the second orbit, the  $\mathbf{E} \times \mathbf{B}$ -drift motion was  
173 confined in the  $x$ - $z$  plane. Because the ambient convection electric field accelerates protons in the  
174  $+z$  direction quickly, the  $z$ -component of the velocity vector of the gyrating proton dominates over  
175 its  $x$ -component. Such particles cannot be observed by SWIM because they do not enter the SWIM  
176 FoV, which is oblique to the motion of these particles.

177 The ion flux on the night side (E) is not simple to interpret. As was mentioned in the  
178 Introduction, there were nightside ion observations by the Apollo lander reported by *Freeman*  
179 [1972], however, more detailed investigations could not be conducted because of the uncertainty of  
180 the upstream solar wind conditions. WIND (*Ogilvie et al. [1996]*; *Mall et al. [1998]*) and NOZOMI  
181 (*Futaana et al. [2003]*) reported lunar-related ions, but these observations were not conducted in  
182 the near lunar wake.

183 Recently, the analysis of the Kaguya data obtained at a height of 100 km identified two  
184 mechanisms of the intrusion of protons into the near lunar wake. The first mechanism is the  
185 acceleration of the solar wind protons into the lunar wake by an electric potential at the wake  
186 boundary (*Nishino et al. [2009a]*). The intrusion takes place at the wake boundary region where the  
187 solar wind velocity vector is perpendicular to the interplanetary magnetic field, with an asymmetry  
188 depending on the Larmor motion of the solar wind protons affected by the large inward electric  
189 field ( $\sim 400$  V). The second mechanism is the transport of the backscattered protons from the  
190 dayside by the  $\mathbf{E} \times \mathbf{B}$ -drift (*Nishino et al. [2009b]*). This intrusion can be realized when the gyro-  
191 radius of backscattered protons is of the same order as the lunar radius. Indeed, the gyro-radii of  
192 protons is  $\sim 1.4 \times 10^3$  km for zero initial velocity under a solar wind velocity of 400 km/s and  
193 magnetic field of 3 nT.



194        However, these theories cannot be applied to explain the night side ion flux observed by  
195 SWIM, which was propagating along the magnetic field. Figure 6 shows the observed velocity  
196 distribution functions for the solar wind (a) sliced in the ecliptic plane and (b) along the direction  
197 perpendicular to the ecliptic plane ( $v_z$ ). The fan-shaped filled pseudo-color image shows the phase  
198 space density of ions observed on the nightside (14:54-15:00 UT), and the contour lines are the  
199 solar wind protons and  $\alpha$ -particles (13:57-14:03 UT). The magnetic field in the solar wind reference  
200 frame estimated from the ACE data is also superimposed on the plot. The cross mark indicates the  
201 solar wind velocity vector from the WIND/SWE data. A relatively large y-component velocity of  
202 the solar wind in SWIM data is probably from instrument effects. The channels where the main  
203 solar wind component are expected have in general lower efficiency than in the ground calibration.  
204 The reasons are yet unknown. There are no such problems in the channels where the nightside flux  
205 was observed. It is clear from Figure 6 (a) that the observed flux is along the direction of the  
206 interplanetary magnetic field, which is different from the Kaguya measurements. The theories to  
207 explain the Kaguya measurements then do not apply. Additionally, it is noted that Figure 6 (b)  
208 shows that we can measure the 3-D velocity distribution function with the assistance of the  
209 spacecraft motion and the nadir pointing.

210        A very simple 1-D model, which is based on the classical theory of a plasma expansion into  
211 vacuum along the magnetic field line, has been employed to explain the plasma distribution in the  
212 lunar wake using an analytical formulation [Ogilvie *et al.* [1996]; Halekas *et al.* [2005]]. Even  
213 though such a 1-D model is too simple for detailed discussions on the physics in the lunar wake, we  
214 use this model to explain the origin of the observed nightside protons (E). Because the solar wind  
215 plasma (both protons and electrons) has higher mobility in the direction parallel to the magnetic  
216 field line than in the perpendicular directions, the solar wind plasma past the terminator  
217 immediately starts filling the lunar wake. In the solar wind rest reference frame, the theory of 1-D

218 expansion into vacuum can be applied to the expansion into the lunar wake. The configuration of  
219 the IMF direction perpendicular to the solar wind velocity vector on 25 January 2009 is favorable  
220 for applying the 1-D expansion theory. Because the pressure gradient is parallel to the magnetic  
221 field direction, the diamagnetic current ( $-\nabla p \times \mathbf{B}$ ) can be neglected.

222 The gyromotion in the direction perpendicular to the magnetic field arising from the thermal  
223 speed may play a role because the gyroradius is  $\sim 100$  km (for protons assuming a thermal velocity  
224 of 30 km and a magnetic field strength of 3 nT), which is comparable to the spacecraft altitude.  
225 However, the gyromotion is less significant compared to the parallel expansion, and we can still  
226 apply the 1-D approximation to this event. The reason is because the gyroperiod ( $\sim 22$  s) is long  
227 enough compared to the travel time of  $\sim 3$  s for the nightside protons from the terminator to the  
228 observation point, and thus the protons experience only a part of the gyration until they are  
229 observed and the trajectory of the protons in the Moon frame does not change significantly.

230 The 1-D formulation of a plasma expansion into a vacuum is summarized by *Samir et al.*  
231 [1983]. The following assumptions are made: a) the electrons are always in equilibrium with the  
232 electrostatic potential employed by Boltzmann's relations (e.g., *Crow et al. [1975]*); b) the solar  
233 wind electrons follow the Maxwell distribution functions with a constant temperature,  $T_e$ , over the  
234 system; c) the ion temperature,  $T_i$ , is zero; and d) charge neutrality. These four assumptions are  
235 rather realistic, but the problematic assumptions that have been introduced for the study of the  
236 plasma expansion into the lunar wake are as follows: e) we neglect of the surface potential; and f)  
237 we ignore the surface absorption. The last two assumptions are quite difficult to include in  
238 analytical models, and therefore, they have been assumed by many authors explicitly or implicitly.

239 The plasma parameters, the ion density ( $n_i$ ), ion velocity ( $v_i$ ), and the electric potential ( $V$ ) can  
240 be described as a function of the distance from the vacuum boundary at the initial state,  $s$ . The set of  
241 the equations could be formulated as:

$$242 \quad n_i = n_e = n_0 \exp\left(-\frac{s}{V_{ia}t} - 1\right) \quad (1)$$

$$243 \quad v = \frac{s}{t} + V_{ia} \quad (2)$$

$$244 \quad V = -\frac{kT_e}{e} \left(\frac{s}{V_{ia}t} + 1\right) \quad (3)$$

245 where  $t$  is time,  $n_0$  is the undisturbed plasma density,  $n_e$  is the electron density,  $e$  is the elementary  
 246 charge,  $M$  is the mass of the proton, and  $k$  is the Boltzmann constant.  $V_{ia}=(kT_e/M)^{1/2}$  is the ion  
 247 acoustic velocity under the assumption of c)  $T_i = 0$ . WIND [Ogilvie et al., 1998] and Lunar  
 248 Prospector [Halekas et al., 2005] observations can be better explained by assuming the solar wind  
 249 electron velocity distribution by a  $\kappa$ -distribution than by a Maxwell distribution. In particular Lunar  
 250 Prospector observations are conducted at an altitude similar to our observation, and the electron  
 251 distributions are consistent with a model using a  $\kappa$ -distribution [Halekas et al., 2005]. Therefore,  
 252 comparison with the  $\kappa$ -distribution is also worthwhile to understand the ion dynamics in the lunar  
 253 wake.

254 Table 1 shows the results of the calculated density and velocity at the spacecraft position. The  
 255 SARA observations show a 2 to 3 times higher velocity than the model calculations. The observed  
 256 density is lower than the model calculations by a factor of 2 to 25. However, the density ratio  
 257 calculated by the 1-D models depends quite sensitively on the solar wind electron temperature,  
 258 which we do not know for this observation. In addition, the density calculation from the  
 259 electrostatic analyzer data is not straightforward. Therefore, we can only say that there is a  
 260 possibility that the observed density ratio is lower than that given by the models. On the other hand,  
 261 the velocity measurement by the electrostatic analyzer is more reliable, and the dependence on the  
 262 models is quite small. Therefore, we can conclude that the observed velocity is significantly  
 263 different from the model. This conclusion may contradict the results of the electron distribution by  
 264 the Lunar Prospector [Halekas et al., 2005]. The contradiction between the electron distribution that

265 is consistent with 1-D model and the observed velocity of the protons higher than the same 1-D  
266 model is yet an open question, but it should be investigated in the future.

267         The reason for the higher velocity (2 to 3 times) of the observed protons is also an open  
268 question. One possible reason is that the 1-D model is too simple to reproduce the lunar wake  
269 plasma physics quantitatively. The ion absorption by the lunar surface, which was neglected in the  
270 models, may potentially explain the higher velocity (and possibly also the lower density) of the  
271 nightside ions. As soon as the solar wind electrons or ions are absorbed by the surface, the self-  
272 similar solutions cannot be used anymore. The theoretical estimate from equation (1) is that  $e^{-1}$   
273 ( $\sim 36\%$ ) of the solar wind ions are absorbed by the lunar surface (see Appendix A). This large  
274 absorption rate may explain the possible lower proton density in the observations. In addition, the  
275 extra acceleration may be explained by the selection effect: only protons with a high velocity  
276 component along the magnetic field can reach the observation point.

277         The surface potential at the terminator region may also play a role [Kimura and Nakagawa,  
278 2008], particularly if one considers the plasma absorption at the lunar surface. Due to the high  
279 speed of the electrons, the solar wind electrons are absorbed by the lunar surface at the terminator  
280 and at the nightside hemisphere of the Moon. Due to the low conductivity of the lunar regolith, the  
281 absorbed electrons are "attached" at the lunar surface, generating the negative surface potential until  
282 the equilibrium of the influx of solar wind electrons and protons is satisfied.

283         Kimura and Nakagawa, 2008 conducted a 2-D particle simulation to investigate the effect of  
284 the surface potential at the terminator. They claim that at the terminator, the electric potential  
285 becomes 60-80V negative due to the electron attachment to the lunar surface. The potential drop  
286 may help accelerate the protons into the wake as observed by SWIM. When they removed the  
287 surface charging effect from their model, the acceleration of the ions decreases less at  $6.5 R_L$ . The  
288 effect of the negative electric potential in the terminator region by the electron attachment may also

289 contribute to the accelerated proton signatures observed by SWIM. However, note that *Kimura and*  
290 *Nakagawa, [2008]* used an unrealistically large Debye length (at most  $R_L/8$ ), and therefore, a direct  
291 comparison with the data from SARA (100 km altitude) is quite difficult. Detailed comparison with  
292 simulation results using more realistic parameters are needed to understand the ion dynamics in the  
293 wake close to the Moon.

## 294 **5. Summary**

295 We analyzed data from the ion spectrometer SWIM on board the Chandrayaan-1 spacecraft  
296 on 25 January 2009. During the observations, the IMF conditions were stable and the geometry of  
297 the upstream electromagnetic field was relatively simple.

298 Three ion populations in addition to the nominal solar wind ions (both protons and  $\alpha$ -  
299 particles) are identified in the SWIM data. On the dayside, backscattered protons and accelerated  
300 backscattered protons are observed, and they are similar to the populations observed earlier by  
301 Kaguya (*Saito et al. [2008]*). These observations can be explained by single particle motions in the  
302 interplanetary magnetic field and the convective electric field.

303 We also detected proton fluxes in the lunar wake region. The observed position was  $\sim 50^\circ$   
304 from the terminator inside the lunar near wake at a height of 100 km. The flux propagates along the  
305 magnetic field in the solar wind frame; therefore, the gyro-motion, interplanetary magnetic field,  
306 and the convective electric field cannot play a role. The proton energy was  $\sim 700$  eV, which was  
307 slightly higher than the solar wind bulk energy of  $\sim 550$  eV during the observation period.

308 The prediction of the 1-D models could not explain the velocity of the observed protons as it  
309 was 2 to 3 times higher than the velocity given by the model. The observed velocity is higher than  
310 the prediction by the models. The reason of the difference in the velocity is yet an open question,  
311 but the surface absorption effect, which is neglected in the analytical models, and the negative

312 surface potential of the Moon at the terminator region and the nightside surface may be one possible  
 313 reason. The absorption of the plasma particles and the resulting large electric potential at the lunar  
 314 surface could be significant for understanding the kinetics of the solar wind ions in the low-altitude  
 315 wake of the Moon.

## 316 **Appendix A. The absorption ratio of protons at the lunar surface**

317 Here we calculate the absorption ratio of the solar wind protons at the lunar surface close to  
 318 the terminator. The coordinate system used in this appendix is drawn in Figure A1. When the solar  
 319 wind protons expand into the lunar wake, a rarefaction wave is formed. The rarefaction wave front,  
 320  $s_{wf}$ , is the boundary separating the undisturbed from the disturbed solar wind. From the equation (1),  
 321 we know that the wave front propagates with a velocity of the ion acoustic speed:

$$322 \quad s_{wf} = -V_{ia} t \quad (A1)$$

323 The total amount of solar wind plasma that is affected by the vacuum expansion,  $N_t$ , is an  
 324 integration of the density as

$$325 \quad N_t = \int_{s_{wf}}^{\infty} n_i ds = n_0 V_{ia} t \quad (A2)$$

326 Conversely, the location of the lunar surface,  $s_{ls}$ , is purely geometric and can be described as

$$327 \quad s_{ls} = R_M - \sqrt{R_M^2 - x^2} = R_M - \sqrt{R_M^2 - (v_{sw} t)^2} \quad (A3)$$

328 The plasma that passes through the lunar surface (in reality, the plasma is absorbed),  $N_a$ , is again an  
 329 integration of the density as follows:

$$330 \quad N_a = \int_{s_{ls}}^{\infty} n_i ds \quad (A4)$$

331 Substituting (5) and (A3) into (A4), the absorbed plasma density is obtained as

$$332 \quad N_a = n_0 V_{ia} t \exp\left(-\frac{S_{ls}}{V_{ia} t} - 1\right) \quad (A5)$$

333 The absorption rate of the solar wind protons at the lunar surface can be calculated as  $N_a/Nt$ . This  
 334 formulation is only valid just after the vacuum expansion starts because the surface absorption  
 335 violates the self-similar solution of (1). Therefore, one must take the limit of the time  $t$  to 0, which  
 336 results in  $N_a/Nt \rightarrow e^{-1}$  ( $t \rightarrow 0$ ).

### 337 **Acknowledgment**

338 We thank the ACE MAG instrument team and the ACE Science Center for providing the  
 339 ACE data. We also thank the WIND/SWE instrument team for the provision of the solar wind  
 340 velocity and the density data. The efforts at the Swedish Institute of Space Physics were supported  
 341 in part by European Space Agency (ESA). The effort at the University of Bern was supported in  
 342 part by ESA and by the Swiss Science Foundation. The efforts at the Space Physics Laboratory,  
 343 Vikram Sarabhai Space Centre were supported by Indian Space Research Organization (ISRO).

### 344 **Reference**

- 345 Barabash, S., A. Bhardwaj, M. Wieser, R. Sridharan, T. Kurian, S. Varier, E. Vijaykumar, V.  
 346 Abhirami, K. V. Raghavendra, S. V. Mohankumar, D. B. Dhanya, S. Thampi, K. Asamura, H.  
 347 Andersson, Y. Fu- taana, M. Holmström, R. Lundin, J. Svensson, S. Karlsson, R. D. Piazza,  
 348 and P. Wurz., Investigation of the solar wind-Moon interaction on board Chandrayaan-1  
 349 mission with the SARA experiment, *Current Science*, 96 (4), 526-532, 2009.
- 350 Bhardwaj, A., S. Barabash, Y. Futaana, Y. Kazama, K. Asamura, D. McCann, R. Sridharan, M.  
 351 Holmström, P. Wurz, and R. Lundin, Low energy neutral atom imaging on the Moon with the  
 352 SARA instrument aboard Chandrayaan-1 mission, *Journal of Earth System Science*, 114(6),  
 353 749-760, doi:10.1007/BF02715960, 2005.

- 354 Birch, P. C., and S. C. Chapman, Particle-in-cell simulations of the lunar wake with high phase  
355 space resolution, *Geophys. Res. Lett.*, 28 (2), 219-222, 2001.
- 356 Crow, J. E., P. L. Auer, and J. E. Allen, The expansion of a plasma into a vacuum, *J. Plasma*  
357 *Physics*, 14 (1), 65-76, 1975.
- 358 Farrell, W. M., M. L. Kaiser, J. T. Steinberg, and S. D. Bale, A simple simulation of a plasma void:  
359 Applications to wind observations of the lunar wake, *Journal of Geophysical Research*, 103  
360 (A10), 23,653-23,660, 1998.
- 361 Freeman, J. W., Energetic ion bursts on the nightside of the moon, *J. Geophys. Res.*, 77 (1), 239-243,  
362 1972.
- 363 Futaana, Y., S. Machida, Y. Saito, A. Matsuoka, and H. Hayakawa, Counterstreaming electrons in  
364 the near vicinity of the moon observed by plasma instruments on board NOZOMI, *J. Geophys.*  
365 *Res.*, 106 (A9), 18,729-18,740, 2001.
- 366 Futaana, Y., S. Machida, Y. Saito, A. Matsuoka, and H. Hayakawa, Moon-related nonthermal ions  
367 observed by nozomi: Species, sources, and generation mechanisms, *J. Geophys. Res.*, 108  
368 (A1), 1025, doi:10.1029/2002JA009366, 2003.
- 369 Futaana, Y., S. Barabash, M. Holmström, and A. Bhardwaj, Low energy neutral atoms imaging of  
370 the moon, *Planet. Space Sci.*, 54 (2), 132-143, 2006.
- 371 Halekas, J. S., S. D. Bale, D. L. Mitchell, and R. P. Lin, Electrons and magnetic fields in the lunar  
372 plasma wake, *J. Geophys. Res.*, 110, A07222, doi:10.1029/2004JA010991, 2005.
- 373 Holmström, M., M. Wieser, S. Barabash, Y. Futaana, and A. Bhardwaj, Dynamics of solar wind  
374 protons reflected by the moon, *J. Geophys. Res.*, in Press, 2010.



- 375 Kallio, E., Formation of the lunar wake in quasi-neutral hybrid model, *Geophys. Res. Lett.*, *32*,  
376 L06107, doi:10.1029/2004GL021989, 2005.
- 377 Kimura, S and T. Nakagawa, Electromagnetic full particle simulation of the electric field structure  
378 around the moon and the lunar wake, *Earth Planets Space*, *60*, 591-599, 2008.
- 379 Lin, R. P., D. L. Mitchell, D. W. Curtis, K. A. Anderson, C. W. Carlson, J. McFadden, M. H. A. na,  
380 L. L. Hood, and A. Binder, Lunar surface magnetic fields and their interaction with the solar  
381 wind: Results from lunar prospector, *Science*, *281* (5382), 1480-1484, 1998.
- 382 Mall, U., E. Kirsch, K. Cierpka, B. Wilken, A. Söding, F. Neubauer, G. Gloeckler, and A. Galvin,  
383 Direct observation of lunar pick-up ions near the moon, *Geophys. Res. Lett.*, *25* (20), 3799-  
384 3802, 1998.
- 385 McCann, D., S. Barabash, H. Nilsson, and A. Bhardwaj, Miniature ion mass analyzer, *Planetary  
386 and Space Science*, *55* (9), 1190-1196, 2007.
- 387 Newbury, J. A., C. T. Russell, J. L. Phillips, and S. P. Gary, Electron temperature in the ambient  
388 solar wind: Typical properties and a lower bound at 1 AU, *J. Geophys. Res.*, *103* (A5), 9553-  
389 9566, 1998.
- 390 Nishino, M. N., K. Maezawa, M. Fujimoto, Y. Saito, S. Yokota, K. Asamura, T. Tanaka, H.  
391 Tsunakawa, M. Matsushima, F. Takahashi, T. Terasawa, H. Shibuya, and H. Shimizu.,  
392 Pairwise energy gain-loss feature of solar wind protons in the near-Moon wake, *Geophys. Res.  
393 Lett*, L12108, doi:10.1029/2009GL039049, 2009a.
- 394 Nishino, N. M., M. Fujimoto, K. Maezawa, Y. Saito, S. Yokota, K. Asamura, T. Tanaka, H.  
395 Tsunakawa, M. Matsushima, F. Takahashi, T. Terasawa, H. Shibuya, and H. Shimizu., Solar-

- 396 wind proton access deep into the near-Moon wake, *Geophys. Res. Lett.*, L16103,  
397 doi:10.1029/2009GL039444, 2009b.
- 398 Ogilvie, K. W., J. T. Steinberg, R. J. Fitzenreiter, C. J. Owen, A. J. Lazarus, W. M. Farrell, and R.  
399 B. Torbert, Observations of the lunar plasma wake from the WIND spacecraft on december  
400 27, 1994, *Geophys. Res. Lett.*, 23 (10), 1255-1258, 1996.
- 401 Russell, C. T., and B. R. Lichtenstein, On the source of lunar limb compressions, *J. Geophys. Res.*,  
402 80 (34), 4700-4711, 1975.
- 403 Saito, Y., S. Yokota, T. Tanaka, K. Asamura, M. N. Nishino, M. Fujimoto, H. Tsunakawa, H.  
404 Shibuya, M. Matsushima, H. Shimizu, F. Takahashi, T. Mukai, and T. Terasawa, Solar wind  
405 proton reflection at the lunar surface: Low energy ion measurement by MAP-PACE onboard  
406 SELENE (KAGUYA), *Geophys. Res. Lett.*, 35, L24205, doi:10.1029/2008GL036077, 2008.
- 407 Samir, U., K. H. Wright Jr., and N. H. Stone, The expansion of a plasma into a vacuum: Basic  
408 phenomena and processes and applications to space plasma physics, *Rev. Geophys.*, 21 (7),  
409 1631-1646, 1983.
- 410 Trávníček, P., P. Hellinger, D. Schriver, and S. D. Bale, Structure of the lunar wake: Two-  
411 dimensional global hybrid simulations, *Geophys. Res. Lett.*, 31, L06102,  
412 doi:10.1029/2004GL022243, 2005.
- 413 Wieser, M., S. Barabash, Y. Futaana, M. Holmström, A. Bhardwaj, R. Sridharan, M. B. Dhanya, A.  
414 Schaufelberger, P. Wurz, and K. Asamura, First observation of a mini-magnetosphere above a  
415 lunar magnetic anomaly using energetic neutral atoms, *Geophys. Res. Lett.*, submitted, 2010.

**416 Figures****417 Figure 1:**

418

419 The CENA and SWIM apertures and the numbering of the viewing directions relative to the  
420 spacecraft (SC) reference frame. The SWIM has a  $\sim 7 \times 160^\circ$  aperture divided into 16 viewing  
421 directions. The CENA aperture is  $10 \times 160^\circ$  divided into seven azimuthal channels. In the nominal  
422 nadir pointing, the spacecraft velocity is parallel to the  $+y_{sc}$  or  $-y_{sc}$  axis, and the  $+x_{sc}$  axis points to  
423 the lunar center.

**424 Figure 2:**

425

426 The energy time spectrograms observed on 25 January 2009 over two consecutive orbits 942 and  
427 943. From top to bottom, the energy-time diagrams for the observed ion counts coming from the  
428 surface (below local horizon), limb (toward the horizon), and space (above the horizon) are shown.  
429 At the top, the time intervals when the spacecraft was in the lunar shadow (eclipse) as well as the  
430 equator crossings are indicated. The spacecraft location (north or south hemisphere) is also  
431 indicated. Five distinct ion populations are identified, and are labeled from A through E.

**432 Figure 3:**

433 The Chandrayaan-1 orbit in the LSE coordinate system (the  $+x$  axis is the Moon-Sun line, the  $+y$   
434 axis the velocity vector of the Sun motion relative to the Moon, and the  $+z$  axis completes the right-  
435 handed system) between 13:30-15:28 UT on 25 January 2009. The orbital period was  $\sim 118$  minutes.

**436 Figure 4:**

437 Interplanetary magnetic field data observed by ACE between 12-18 UT on 25 January 2009.  
438 Considering the propagation time from ACE to the Moon of 1 hour, the solar wind at the Moon  
439 corresponds to 13-19 UT (upper axis). From top to bottom: the magnitude, the latitudinal  
440 component, and the longitudinal component in the GSE frame of the magnetic field are displayed.

441 **Figure 5**

442 Illustration of the proton transport by the gyromotion under the two different upstream magnetic  
443 field directions (a)  $135^\circ$  and (b)  $90^\circ$ . The illustration is seen from the north pole (i.e., projection to  
444 the  $x$ - $y$  plane). The SWIM FoV is drawn at the north pole for simplicity. At the north pole, the  
445 acceptance is only  $10^\circ$  degrees under the nadir pointing. (a) If the IMF direction is  $135^\circ$ , the IMF is  
446 almost in the same plane as the orbital plane of the observation. Therefore, the ExB drift is  
447 perpendicular to the orbital plane, and SWIM may be able to see the gyrated protons. (b)  
448 Conversely, when the IMF direction becomes  $90^\circ$ , the gyration is only in the  $x$ - $z$  plane; therefore,  
449 SWIM cannot detect the gyrated protons at all.

450 **Figure 6:**

451 (a) Velocity distribution functions of the solar wind (contour lines) and the nightside ions (filled  
452 polygons) in the lunar ecliptic plane. The velocity distribution functions of solar wind ions and the  
453 nightside ions are the average of the observation between 13:57-14:03 and 14:54-15:00 UT,  
454 respectively. During the period, the field of view of SWIM is in the ecliptic plane. The velocity of  
455 the solar wind from WIND/SWE data is shown by the cross. The magnetic field line is  
456 superimposed in the solar wind reference frame. (b) The solar wind velocity distribution as a  
457 function of  $V_z$ . The  $V_z$  component can be measured by the assist of the spacecraft motion and its  
458 nadir pointing. The data were taken between 13:55 and 14:05 UT.

459 **Figure A1.**

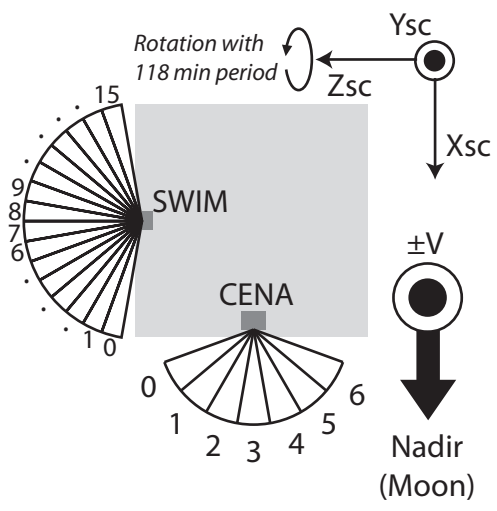
460 The coordinate system used for the calculation of the absorption rate. The  $x$ -axis is the Moon-Sun  
461 line identical to the LSE frame. The  $s$ -axis is perpendicular to the  $x$ -axis along the magnetic field,  
462 but its origin is the wake boundary at the terminator. The rarefaction wave front and the lunar  
463 surface are drawn by dashed lines.

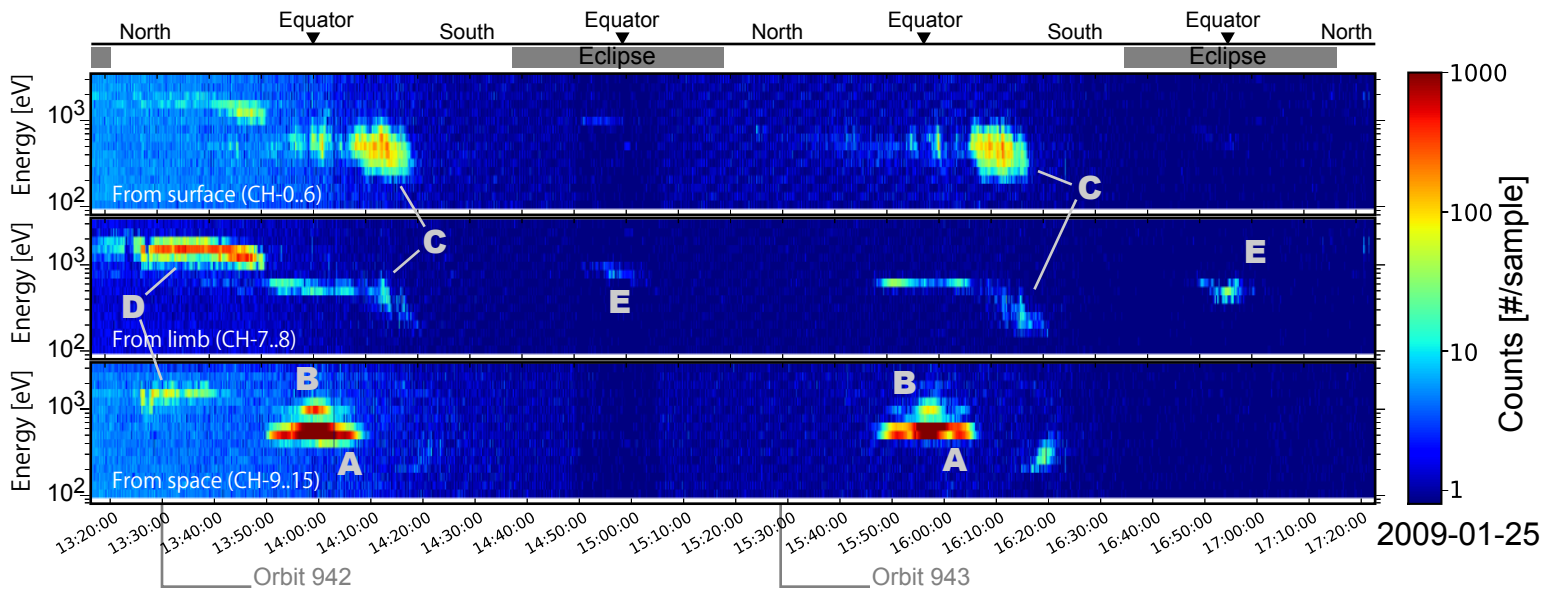
464

465 Table 1: Summary of the calculation. \*1 Taken from Newbury et al., 1998. \*2 Taken from  
 466 Halekas et al., 2005.

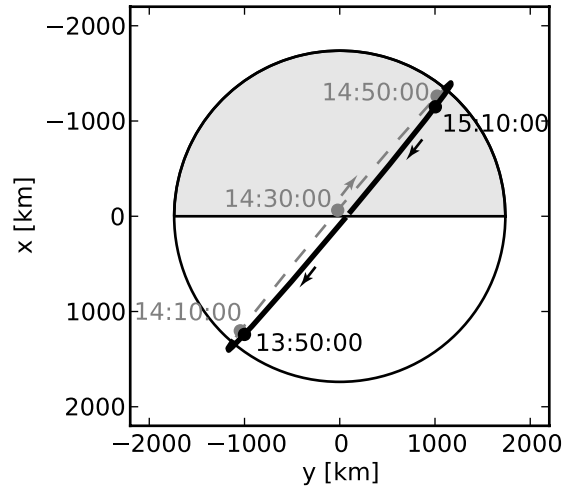
	Velocity	Density (ratio)
SARA observation	300-400 km/s	0.05-0.2%
Model by Maxwellian electrons [Samir et al. (1983)] Te=141000±38000 K <sup>*1</sup>	161-170 km/s	0.4-1.2%
Model by $\kappa$ -distribution [Halekas et al. (2005)] Te=141000K <sup>*1</sup> ; $\kappa=4.5$ <sup>*2</sup>	185 km/s	0.9%

467





View from North



View from Sun

